Journal of Alloys and Compounds 509 (2011) 8700–8706

Contents lists available at ScienceDirect

Journal of Alloys and Compounds

journal homepage: www.elsevier.com/locate/jallcom

Ionic compounds lamination reaction and characteristics of photosensitive copper indium sulfide on titania nanotube arrays

Horng-Yi Chang[a,*], Wei-Jei Tzeng[a], Chia-Hsin Lin[b], Syh-Yuh Cheng[b]

[a] Department of Marine Engineering, National Taiwan Ocean University, Keelung 20224, Taiwan, ROC
[b] Ceramic Microengineering Laboratory, Material and Chemical Research Laboratories, Industrial Technology Research Institute, Chutung 31060, Taiwan, ROC

ARTICLE INFO

Article history:
Received 16 April 2011
Received in revised form 4 June 2011
Accepted 6 June 2011
Available online 23 June 2011

Keywords:
TiO_2 nanotube arrays
Photosensitive $CuInS_2$
Stoichiometry
Ionic compounds lamination reaction (ICLR)

ABSTRACT

This study investigates using an inorganic photosensitive $CuInS_2$ (CIS) coating instead of an organic dye on TiO_2 nanotube arrays (TNAs). The stoichiometric characteristics by use of various deposition parameters such as precursor concentrations (0.1 M, 0.05 M, and 0.01 M) and deposition cycles (1–60 cycles) are then analyzed in relation to the crystallinity and photosensitivity. TNAs are synthesized by anodic oxidation of Ti metal, modified by the TiO_2 film, and are subsequently annealed at 450 °C for 30 min, producing what are named T-TNAs. They show high photocatalytic efficiency and photosensitivity under UV-illumination. The photosensitive CIS coatings on the T-TNAs are processed by an ionic compounds lamination reaction (ICLR) method. The more immersion cycles and the higher the precursor concentration of copper sulfide, the more CIS peeled off as precipitates formed, which result in less indium sulfide deposition being required for reacting with the copper sulfide to reach stoichiometry. Near stoichiometric CIS can be obtained by controlling the precursor concentration and deposition cycles of the ICLR process. Good crystallinity and n-type characteristics are achieved by controlling the precursor concentrations and deposition cycles suitably to obtain a high current density. When the Cu/In ratio is adjusted for n-type characteristics, the current density reaches at least 300 $\mu A/cm^2$ under visible light illumination intensity of 100 mW/cm^2.

1. Introduction

Inorganic photosensitizers with a narrow band gap have attracted much interest in the solar cell industry. Copper indium sulfide ($CuInS_2$) is regarded as an efficient inorganic photosensitive material for photovoltaic solar cells [1] because it has a direct band gap of 1.5 eV, which matches the solar spectrum, and a large absorption coefficient ($\alpha \sim 10^5\ cm^{-1}$) [2]. $CuInS_2$ (CIS) is environmentally friendly and less toxic than other II–VI semiconductors, including CdTe, CdSe, or I–III–VI_2 semiconductors such as $CuInSe_2$, $CuGaSe_2$. The CIS photosensitive material displays an n-type (Cu/In < 1) or a p-type (Cu/In > 1) semiconductivity depending on the Cu/In ratio. Numerous synthetic methods exist for synthesizing an excess amount of copper for a p-type CIS [3–6]. An excess amount of copper results in a p-type CIS and a Cu_2S layer at the surface of the particles or films. A chemical treatment to reduce the excess copper results in an n-type semiconductivity and leads to the formation of an In_2S_3 layer at the surface [7–9].

The phase composition and structure of the CIS depend on the growth mechanism and the Cu/In ratio in the synthesis processes. There are many crystalline phases for CIS synthesis, including polymorphisms of chalcopyrite, sphalerite (zinc-blend), wurtzite as well as ordered copper–gold, and copper–platinum structures [8–14]. A variety of chemical solution approaches for synthesizing CIS nanostructures have been reported, such as molecular source [15], colloid and hydro/solvothermal methods [16–18], microwave heating [19], and surfactant-assisted chemical reactions [18,20]. Many nanocrystal morphologies such as spherical, hollow and pyramidal nanocrystals, nanorods, nanoribbons, nanowires, nanotubes and porous microspheres have a significant correlation with the synthesizing parameters, including the use of solvents and surfactants, concentrations, temperatures as well as pH values [12,14,16,18,21,22].

The discontinuous adhesion interface of the transparent conductive oxide (TCO) substrate and the TiO_2 nanoparticle network in dye-sensitized solar cells (DSCs) generally form a barrier for electrons transferring from TiO_2 to TCO. Additionally, TCO has a large resistance compared with the metal (Ti), increasing the energy consumption. By contrast, the organic dye coating on the TiO_2 surface can decompose easily under solar irradiation. TiO_2 nanotube arrays (TNAs) were fabricated by anodic oxidation [23] to obtain a high aspect ratio. This kind of one-dimensional structure not only

* Corresponding author. Tel.: +886 2 24621292x7103, fax: +886 2 24633765.
E-mail address: hychang@mail.ntou.edu.tw (H.-Y. Chang).

0925-8388/$ – see front matter © 2011 Elsevier B.V. All rights reserved.
doi:10.1016/j.jallcom.2011.06.018

provides a higher surface area, but also offers a more direct route for electrons to transfer from TiO_2 to the electrode, making it superior to the TiO_2 nanoparticle network.

An extremely thin absorber (ETA) coating in a 3D-particulate network is applied to try to replace the organic photoabsorber [24]. The CIS using atomic layer chemical vapor deposition (AL-CVD) was used for 3D nanocomposite solar cells [25]. A low-cost chemical bath deposition (CBD) method to further facilitate the ETA coating of nanotubes was also studied intensively [26]. The CIS and Cu_xS films were also prepared on other substrates such as glass, indium tin oxide (ITO) glass and silicon wafers. They were prepared by ionic reactions in an alkaline chemical bath [27], chemical deposition with sequential immersion of the substrate [28], and a successive ionic layer absorption and reaction (SILAR) method, which immersed the substrate in different cationic and anionic precursor solutions, rinsing before every immersion with de-ionized water to remove the loosely bounded species [29,30]. Those results reveal the nanocrystallinity of the CIS thin films. The electrical resistivity is of the order of 10 Ω cm for CIS films. Depending on the processing conditions, the prepared CIS films were either Cu-rich or In-rich, showing p-type or n-type electrical conductivity, respectively.

However, the inorganic photosensitive CIS coating on the TNAs prepared by our modified successive ionic layer absorption and reaction method, indicated to as the ionic compounds lamination reaction (ICLR) method, and the resulting photosensitive properties, have not yet been investigated. In this work, the defective surface of the TiO_2 nanotubes is modified by titania thin film to promote the crystallinity and to provide a more suitable surface for CIS deposition resulting in more stable photosensitivity under visible light illumination. This study investigates the deposition behavior and coverage morphology of CIS on the TNAs as well as their stoichiometric formation with respect to their photosensitive properties.

2. Experimental details

The electrochemical process of the anodization system consisted of a two-electrode configuration that was used to prepare the titania nanotube arrays (TNAs). Titanium foil with an area of 2.0 cm × 1.0 cm and a thickness of 150 μm was used as the anode. A platinum sheet (99.99%) was used as the cathode. The electrolyte composition in the anodization was 0.3 wt% NH_4F (98%, RDH) dissolved in ethylene glycol (99.5%, RDH) with the addition of 2–3 vol% of de-ionized water (D.I.-H_2O). Anodic oxidation was performed using a dual-range DC power supply (GWINSIEK Co., SPD-3606). The anodization potential was applied at 60 V for 1–2 h.

After anodic oxidation, the as-anodized specimens were washed in a bath of D.I.-H_2O and dried using nitrogen gas. The dried specimens were annealed at 450 °C for 30 min and then ultrasonically cleaned for 5 min. The annealed TNAs were then immersed in a 0.1 M titanium chloride (98%, Fluka) ethanolic solution and de-aired ultrasonically for 60 s. After being de-aired, the TNAs remained in the 0.1 M titanium chloride for 24 h, and were then washed with water and dried using nitrogen gas. The $TiCl_4$ coating was transformed into a TiO_2 modification layer on the nanotube by heat-treatment at 450 °C for 30 min. An inorganic photoabsorption layer $CuInS_2$ (CIS) was deposited onto the TiO_2 modified TNAs using an ICLR method. The precursors were $InCl_3$ (99.99%, Alfa Aesar), $CuCl_2$ (98%, SHOWA) and $Na_2S{\cdot}9H_2O$ (98%, Sigma–Aldrich). The concentration of the precursors $InCl_{3(aq)}$, $CuCl_{2(aq)}$ and $Na_2S_{(aq)}$ all varied between 0.1 M, 0.05 M, and 0.01 M. The ICLR procedure followed the immersion of the TiO_2 modified TNAs (named the T-TNA) substrate. This was first performed in $CuCl_{2(aq)}$ ultrasonically for 30 s, followed by ultrasonic cleaning in D.I.-H_2O for 30 s, and then in $Na_2S_{(aq)}$ ultrasonically for 30 s, followed by ultrasonic cleaning in D.I.-H_2O for 30 s. This process was repeated over many cycles to form Cu_xS ($1 \le x \le 2$). The repeated cycles were named CuSa; for example, CuS10 represents 10 deposition cycles of $CuCl_{2(aq)} \rightarrow H_2O \rightarrow Na_2S_{(aq)} \rightarrow H_2O$ on the T-TNA substrate. After the above ICLR procedure to form CuSa deposition, immersed the CuSa treated T-TNA substrate in $InCl_{3(aq)}$ ultrasonically for 30 s, followed by ultrasonic cleaning in D.I.-H_2O for 30 s, and then immersed in $Na_2S_{(aq)}$ ultrasonically for 30 s, followed by ultrasonic cleaning in D.I.-H_2O for 30 s, forming In_yS. The repeated cycles were named InSb deposition; for example, InS9 represents 9 deposition cycles of $InCl_{3(aq)} \rightarrow H_2O \rightarrow Na_2S_{(aq)} \rightarrow H_2O$ on the CuSa. We combined CuSa and InSb to complete the lamination of the CIS layer. The laminated layers were then further dried at 80 °C for 30 min on a hot-plate and post-annealed at 450 °C for 1 h in an electrical furnace.

The crystal structure was characterized by X-ray diffraction (XRD, Panalytical X'Pert Pro MPD). All the microstructures and the morphology of the deposited nanotubes were determined using a field emission-scanning electron microscope (FE-SEM, Hitachi Field-Emission S-4800), and the CIS elemental analyses were performed by EDXA (energy dispersive X-ray analysis). The microstructure and composition of the nanotube cross-sections were determined using a field emission-transmission electron microscope (FE-TEM, JEOL JEM-2100F) and EDXA. The copper and indium content were analyzed with the precursor solution and the after-deposited solution of $CuCl_{2(aq)}$ and $InCl_{3(aq)}$, respectively, using an inductively coupled plasma-optical emission spectrometer (ICP-OES, Spectro Spectroflame-P). The photocatalytic activity of the TNAs and T-TNAs was measured by the decomposition of 0.01 ppm methylene blue (MB). The photocatalytic activity of MB irradiated by a 365 nm wavelength UV light (UV Lamp, UVP UVGL-58) was characterized by a UV–visible spectrophotometer (Jasco V-630). The absorption spectra were measured in the wavelength range of 400–700 nm. The photosensitivity of the T-TNAs and the CIS deposited T-TNAs was determined by measuring the photocurrent density under visible light illumination, generated by a Xenon lamp (Khlamp KHX-13 W) with a visible light filter, irradiating the photoanodes immersed in the 0.1 M NaOH electrolyte with a two-electrode configuration.

3. Results and discussion

3.1. A good substrate of TiO_2 nanotube arrays for photosensitive $CuInS_2$ deposition

The typical morphology of TiO_2 nanotube arrays (TNAs), prepared with a water content of 2 vol%, 60 V–10 mA/cm^2 anodization maintained for 2 h, and post-annealing at 450 °C for 30 min, is shown in Fig. 1(a). It reveals that the TNAs had a diameter of 100–120 nm and a tube wall thickness of 20–30 nm. Regular nanotube arrays grew vertically from the titanium metal substrate. The FE-TEM image in Fig. 1(b) also shows the nanotubes in parallel but with slightly helical and twisted geometries. The selective area electron diffraction (SAED) pattern shown in the insert in Fig. 1(c) indicates that the titania nanotube has polycrystalline characteristics. The average crystal size (D) in the nanotubes is about 20 nm, as calculated by the FWHM (full width at half maximum, B) of the most intense X-ray diffraction peak (1 0 1), $2\theta = 25.3°$, of the anatase using the Scherrer equation ($D = 0.9\lambda/B \cos\theta$, where λ is the X-ray wavelength of 1.5406 Å).

An anatase phase with a high crystallinity and nano-sized grains as well as a large surface area is a necessary requirement for a TiO_2 photocatalyst. Fig. 2(a) shows that the methylene blue was decomposed efficiently by the annealed TiO_2 nanotube arrays by anodization at 60 V for 2 h. The high photocatalytic effect of the annealed nanotube arrays reveals well-crystallized nanotubes with a large surface area. It is proposed that the photocatalytic effect is then enhanced by the growth of vertically oriented nanotubes, 100 nm in diameter average, and composed of a pure anatase phase.

The atomic percentages of titanium and oxygen over the cross-sectional fracture surface of the $TiCl_{4(aq)}$ modified TiO_2 nanotube (T-TNA) exhibit some composition fluctuation, as shown in Fig. 1(d). The atomic ratio of titanium (Ti) to oxygen (O) appears to be nonstoichiometric around the nanotube wall region, as indicated by a line scanning length from 25 nm to 45 nm, according to EDXA (Fig. 1(d)). This nonstoichiometric deviation around the nanotube wall, which only exhibited a nano-coating of $TiCl_4$ on the nearly 20 nm thick TiO_2 nanotube wall (also see Fig. 1(c)), is the result of a geometrically uneven fracture surface of the nanotube wall. The T-TNAs further improved the decomposition efficiency of the MB by up to 90%. Such a modification by the thin coating of titania derived from $TiCl_4$ also resulted in an improvement in the photocurrent density under UV irradiation (Fig. 2(b)). It shows that the photocurrent density using the TiO_2 (or $TiCl_4$) modified TNAs is higher than that using only the annealed TNAs without a TiO_2 coating. This indicates that the defects (if any) that existed on the surfaces of the titania nanotubes were modified by the TiO_2 coating to reduce the trap of transferring electrons. However, when the

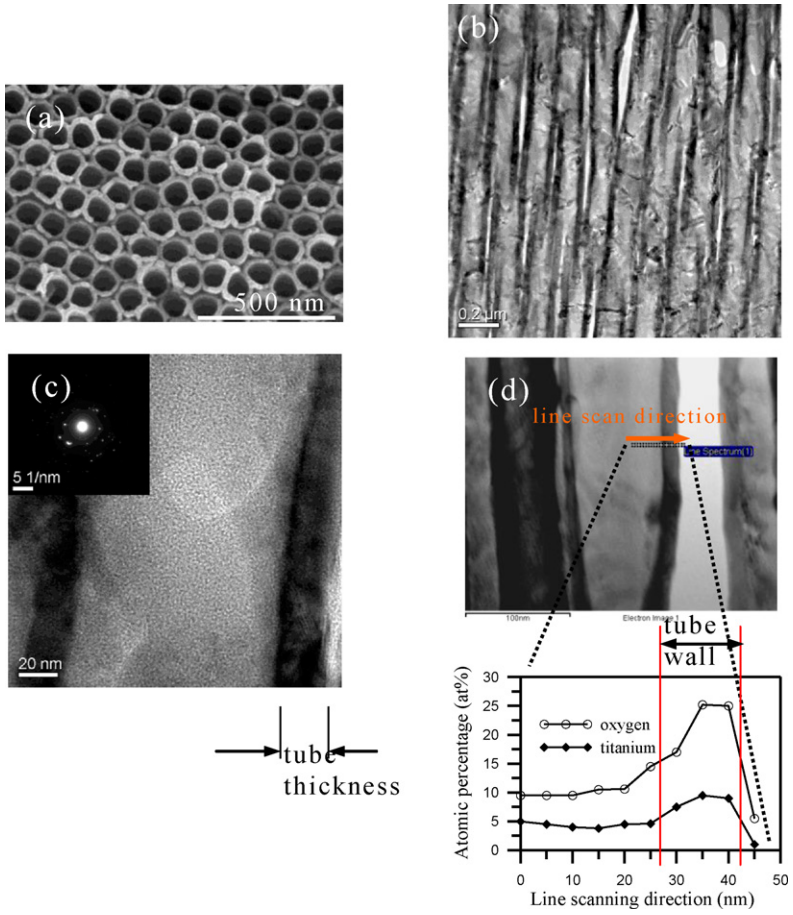

Fig. 1. Micrographs of TiO_2 nanotube arrays (TNAs), (a) top morphology by FE-SEM, (b) cross-sectional surface by FE-TEM, (c) nano-grains in single nanotube by FE-TEM (inset is SEAD pattern), and (d) cross-sectional surface and elemental profile of oxygen and titanium by line scanning analysis.

T-TNAs were examined in a two-electrode electrochemical bath under visible light illumination, a photocurrent response could not be detected. This is an indication that the band gap of the anatase is in UV energy range. The result demonstrates that the photosensitive response to visible light after the $CuInS_2$ coating is actually due to the photosensitive behavior of $CuInS_2$.

The photo-generated electrons released by the UV light may be transported along an almost straight route in the TiO_2 nanotube without the contact barriers of three dimensional TiO_2 nanoparticles network. Thus, the photocatalytic and photosensitive efficiency are enhanced by T-TNAs. These results allow for well-crystallized TiO_2 nanotube arrays to be used as substrates with $CuInS_2$ (CIS) photosensitive materials deposited by the ICLR process.

3.2. Characterization of $CuInS_2$ deposition by ionic compounds lamination reaction

In our study, the CIS layers deposited on the T-TNAs by the conventional SILAR method ($CuCl_2 \rightarrow Na_2S \rightarrow InCl_3 \rightarrow Na_2S$) show a various morphology and particle shape depending on the pH values of the precursor solution. When an acidic precursor solution was used, for example at pH 4.3, the CIS layers comprised nano-spherical particles smaller than 20 nm in diameter but with aggregation, as shown in Fig. 3(a). When an alkaline precursor solution was used, for example at pH 10, the CIS layers mainly comprised thin flakes mixed with a few nano-spherical particles, as shown in Fig. 3(b). In accordance with our experimental results, indium sulfide precipitation displayed a flake morphology in an

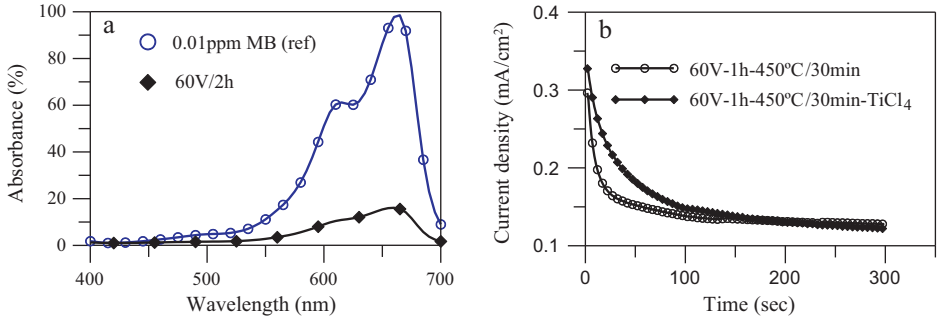

Fig. 2. Photocatalytic and photosensitive characteristics of TNAs, (a) annealed TNAs behaves high photocatalytic efficiency for methylene blue (MB), (b) $TiCl_4$ modified TNAs (T-TNAs) exhibits higher photocurrent density than only annealed TNAs.

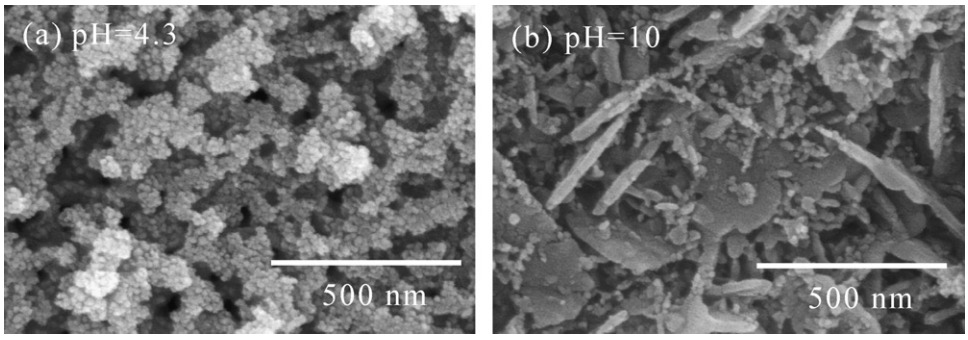

Fig. 3. FE-SEM micrographs of CIS layers deposited on T-TNAs with different pH values of precursor concentration in conventional SILAR process, (a) pH 4.3, (b) pH 10.

alkaline indium precursor solution. The spherical particles indicated the rapid nucleation and formation of species in the acidic environment. The elemental analyses of EDXA showed far less indium than copper in the CIS particles using the conventional SILAR method.

However, the SILAR method, first reported in mid-1980s [31], is relatively simple, quick, economical and suitable for the large area deposition of any configuration. In our work, the heterogeneous nucleation and growth of CIS on T-TNAs was obtained using a precursor solution maintained at pH 4.3 but modified using the SILAR method; the ICLR process was then developed.

The atomic ratio of Cu/In decreases with an increasing number of InSb deposition cycles, even when the precursor concentration changes from 0.1 M to 0.01 M in the ICLR process, as shown in Table 1 and Fig. 4. The likely reason is that the indium increases on the copper sulfide CuS10 and CuS20 in Fig. 4 from lamination by indium sulfide during each InSb deposition cycle. The more immersion cycles of InSb that were performed, the greater is the amount of copper sulfide and indium sulfide lamination that may occur in the ICLR process. After post annealing, those copper sulfide and indium sulfide laminations reacted to form copper indium sulfide due to the rapid diffusion of Cu [24]. Stoichiometric $CuInS_2$ could be reached by controlling the precursor concentration and deposition cycles of the ICLR process, such as the samples of 0.01 M CuS10InS4, 0.05 M CuS10InS6 and 0.1 M CuS10InS7, shown in Fig. 4. The results of the same ratio of Cu/In for different concentration in Fig. 4 indicate that a high copper precursor concentration requires more deposition cycles of indium sulfide for the same number of copper precursor deposition cycles, such as CuS10.

The heterogeneous deposition of copper sulfide occurred around the edge of the open end of the TiO_2 nanotube. A low formation activation energy of Cu_xS is required around the uneven top open hole of the nanotubes. The subsequent nucleation and growth that proceeds peripherally along the top open hole of the nanotubes pile the CIS nanoparticles into a crater-like shape. Thicker deposition on the nanotube surface is obtained using a higher precursor concentration. The comparison is shown in Fig. 5(a) and (b), and the 0.1 M deposition is thicker than the 0.05 M deposition of the CIS for the same CuS10InS7. The crater deposition behavior progressed independently of the different precursor concentration and deposition cycles. The number of indium sulfide deposition cycles, in the range of 10–15, that reacted with the copper sulfide deposition layers reached a constant Cu/In ratio for CuS10 with different precursor concentrations of 0.1 M and 0.01 M. This constant Cu/In ratio results in In-rich CIS (Fig. 4).

Using the precursor concentration of 0.05 M as an example, the more copper sulfide deposition cycles, such as CuS20, on the T-TNAs surface, the more deposition cycles of indium sulfide, such as InS12, are required to reach the stoichiometric CIS, as shown in Fig. 4 and Table 1. By contrast, less deposition or coverage of the CIS particles on T-TNAs for a dilute precursor concentration of 0.01 M is further observed in Fig. 5(c). However, even an increase in the number of deposition cycles up to CuS40 does still not provide enough coverage of grown CIS particles on the T-TNAs for InS7 deposition. When compared with a high copper precursor concentration (0.1 M), the same InS7 exhibits a thick and aggregate coverage on the T-TNAs, as shown in Fig. 5(a). Therefore, it is necessary to use a suitable

Table 1
The atomic ratio of Cu/In according to EDXA of various InSb deposition cycles for 10 deposition cycles of Cu_xS (CuS10) in different precursor concentrations (0.01–0.1 M) and for 20 deposition cycles of Cu_xS (CuS20) in precursor concentration 0.05 M specially.

Samples\Stoichiometry	Cu	In	S	Cu/In
0.1 M CuS10InS5	1.75	0.71	2	2.46
0.1 M CuS10InS7	0.94	0.8	2	1.18
0.1 M CuS10InS9	0.33	0.92	2	0.36
0.1 M CuS10InS10	0.59	0.97	2	0.61
0.1 M CuS10InS15	0.28	1.11	2	0.25
0.1 M CuS10InS20	0.19	1.23	2	0.15
0.05 M CuS10InS5	1.48	1.02	2	1.45
0.05 M CuS10InS6	0.95	1.10	2	0.86
0.05 M CuS10InS7	0.92	0.98	2	0.94
0.05 M CuS10InS9	0.79	0.96	2	0.82
0.05 M CuS10InS10	0.37	1.12	2	0.33
0.01 M CuS10InS2	2.29	1.39	2	1.65
0.01 M CuS10InS3	1.83	1.56	2	1.17
0.01 M CuS10InS4	2.45	1.87	2	1.31
0.01 M CuS10InS7	0.36	1.72	2	0.21
0.01 M CuS10InS9	0.47	1.48	2	0.32
0.01 M CuS10InS10	0.41	1.44	2	0.28
0.05 M CuS20InS6	2.26	0.64	2	3.53
0.05 M CuS20InS8	1.88	0.65	2	2.89
0.05 M CuS20InS10	1.96	0.82	2	2.39
0.05 M CuS20InS12	0.86	0.81	2	1.06

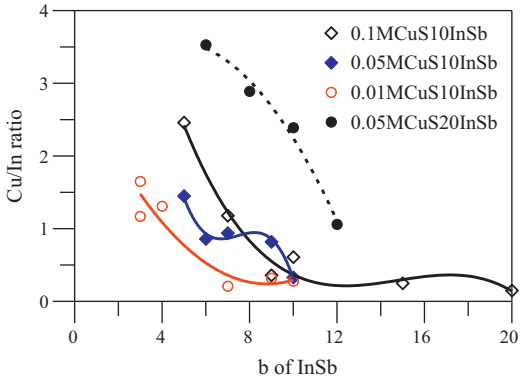

Fig. 4. The ratio of Cu/In as the function of InSb for different precursor concentration and deposition cycles of CuSa.

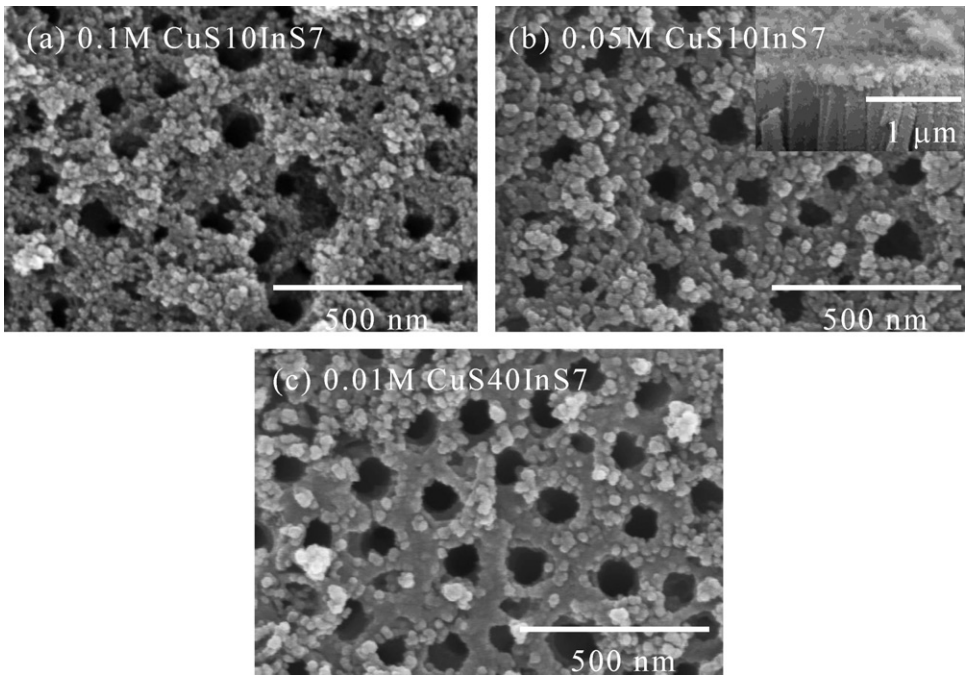

Fig. 5. FE-SEM micrographs of CIS layers deposited on T-TNAs with different precursor concentration and deposition cycles in ICLR process, (a) 0.1 M CuS10InS7, (b) 0.05 M CuS10InS7, (c) 0.01 M CuS40InS7. The inset in (b) is cross-sectional area of 0.05 M CuS10InS7.

precursor concentration such as 0.05 M to achieve homogeneous coverage and a suitable thickness of the CIS layer to compensate for crater formation, as shown in Fig. 5(b). Most of CIS nanoparticles were deposited on the surface around the open end of the TiO_2 nanotubes with few particles entering into the interior as observed in Fig. 5(b) and its inset. The difficulty depositing onto the top smooth surface region and interior wall of the TiO_2 nanotubes may be that they provide too high formation activation energy to CIS nanoparticle nucleation compared to the uneven edge of the open hole.

The more deposition cycles of copper precursor (CuSa) that were performed, the more immersion cycles of InSb should be necessary to reach the stoichiometric CIS. For example, the deposition cycles of 0.05 M copper sulfide CuS20 require InS12 compared with 0.05 M CuS10InS7, as shown in Table 1 and Fig. 4. For the same number of deposition cycles of copper sulfide, such as CuS10 shown in Fig. 4, a precursor concentration higher than 0.05 M is necessary to reach the ratio of (Cu/In) = 1. However, the number of deposition cycles of InSb was not equal to the number of deposition cycles of CuSa, for example, 0.05 M CuS10InS7 for (Cu/In) ~ 1. The deposited CIS nanoparticles were observed to peel off the top surface of the nanotubes to become precipitates at a higher precursor concentration when too many CuSa deposition cycles were carried out, for example, 0.05 M CuS30. This phenomenon was also observed by Sartale and Lokhande [30]. From the ICP-OES results in Table 2, the elemental analyses show that the original precursor concentration before deposition was 0.0474 M for the as-prepared 0.05 M $InCl_{3(aq)}$. The difference in the data between the analyzed ICP-OES (0.0474 M) and the as-prepared (0.05 M) solution of $InCl_{3(aq)}$ is believed to be due to human error in the reagent preparation. The result does not affect the trend of the following comparisons. From Table 2, an obvious decrease in the amount of indium to 0.0460 M after ICLR process is observed. That is, the amount of indium that was no longer in the precursor solution went into the CIS formation of the CuS30InS15 lamination. However, the analysis of the precipitates shows the CIS nanoparticles. It indicates a ratio of Cu/In > 1 in the precipitates, meaning that copper was lost during the InSb deposition. That is why the number of deposition cycles of InSb is always less than that of CuSa to obtain the stoichiometric CIS. By contrast, a significant amount of indium that redissolved into the ICLR solution can be observed from the ICP-OES result, for example, the InS30CuS15 after-deposited solution in Table 2. When first using CuS30, and subsequently depositing InS15, the copper redissolved into the ICLR solution due to thermodynamic equilibrium but was not noticeable compared to the redissolution of indium when first using InS30, and subsequently depositing CuS15. It may be that the adsorption energy of copper sulfide is lower than that of indium sulfide on the T-TNAs substrate. That may result in the more amounts of indium redissolution into the ICLR solution. This requires further study in the future. The reason we first used the CuSa deposition and then the InSb deposition to prepare the CIS was based on these results. When the number of deposition cycles of CuSa increased, the atomic ratio of Cu/In became larger than 1 as shown in Fig. 4. Furthermore, the atomic ratio of Cu/In was approximately equal to 1 as the InSb increased, as indicated by 0.05 M CuS20InS12. The coverage and thickness of the CIS layers did not appear to change significantly with an increase in the CuSa and InSb for the same precursor concentration, for example at 0.05 M, because more CIS precipitates may occur from the deposition layers.

Table 2
The elemental analyses of $InCl_{3(aq)}$ and $CuCl_{2(aq)}$ original solution and after ICLR processed solution by ICP-OES.

Samples	Cu (mol/l)	In (mol/l)
0.05 M $InCl_3$ original precursor solution		0.0474
CuS30InS15 after-deposited solution	1.10×10^{-5}	0.0460
CuS30InS15 precipitates	1.73×10^{-4}	1.56×10^{-4}
0.05 M $CuCl_2$ original precursor solution	0.0517	
InS30CuS15 after-deposited solution	0.0491	1.22×10^{-4}

The CIS crystallinity increased as the precursor concentration increased from 0.05 M to 0.1 M, as shown in Fig. 6(a) and (b). Although the increase in the number of deposition cycles of CuSa and InSb could increase the crystallinity of the CIS, second phases occurred such as in 0.05 M CuS40InS18 in Fig. 6(c). This may result from a significant number of CIS nanoparticles peeling off due to

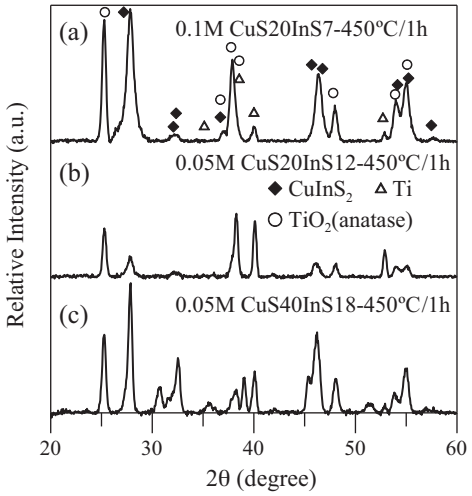

Fig. 6. X-ray diffraction patterns of different precursor concentrations and deposition cycles after 450 °C/1 h annealing, (a) 0.1 M CuS20InS7, (b) 0.05 M CuS20InS12 and (c) 0.05 M CuS40InS18.

loose adhesion resulting from lamination that was too thick as to changing the ratio of Cu/In. Therefore, the precursor concentration determined the coverage and thickness as well as the crystallinity but the number of deposition cycles of CuSa and InSb determined the phase purity and Cu/In ratio of CIS.

3.3. Properties evaluation of $CuInS_2$ deposited photoanode

When the CIS coated T-TNAs photoanode was irradiated by visible light, the current density increased as the number of deposition cycles of InSb increased for a fixed CuS10 in one precursor concentration, as shown in Fig. 7(a)–(c). The figures show that a higher current density is obtained for Cu/In < 1 such as 0.1 M CuS10InS9 and CuS10InS10 in Fig. 7(a) as well as 0.05 M CuS10InS10 in Fig. 7(b). When an indium rich phase was achieved in CIS using a dilute precursor concentration such as 0.01 M, there was no obvious difference among current densities for CuS10InS7–10, as shown in Fig. 7(c) (also refer to Fig. 5(c) showing too low film coverage and thickness not enough). A Cu/In ratio of less than 1 results in an n-type $CuInS_2$ semiconductor. The n-type characteristic improves electron emission under visible light irradiation such as with an organic dye. From the above results, insufficient coverage and thickness as well as the crystallinity of the CIS affected the intensity of the current density, as seen in Figs. 5(c), 6(b) and (c) and 7(c). Therefore, controlling the precursor concentration and deposition cycles suitably could increase the adhesion and coverage on T-TNA substrate to obtain a satisfactory CIS film thickness and crystallinity, as shown in Figs. 5(b) and 6(a) and (b). A Cu/In ratio of less than 1 even nonstoichiometric $CuInS_2$ in the ICLR prepared nanoparticles can exhibit a high current density of at least 300 $\mu A/cm^2$ under visible light illumination with 100 mW/cm^2 by controlling the precursor concentration and deposition cycles of CuSa and InSb, as shown in Fig. 7(a) and (b).

In summary, the crystallinity and photosensitivity of photoanode intimately correlated with the CIS film thickness. The thickness depended on the precursor concentration and deposition cycles. These presented results proved that the concentration of the precursor solution determined the stoichiometry, coverage and thickness of CIS layer. Sufficient amounts of copper and indium ions in the deposition cycles could affect the crystallinity and stoichiometry of CIS. Too many deposition cycles of CuSa and InSb induced

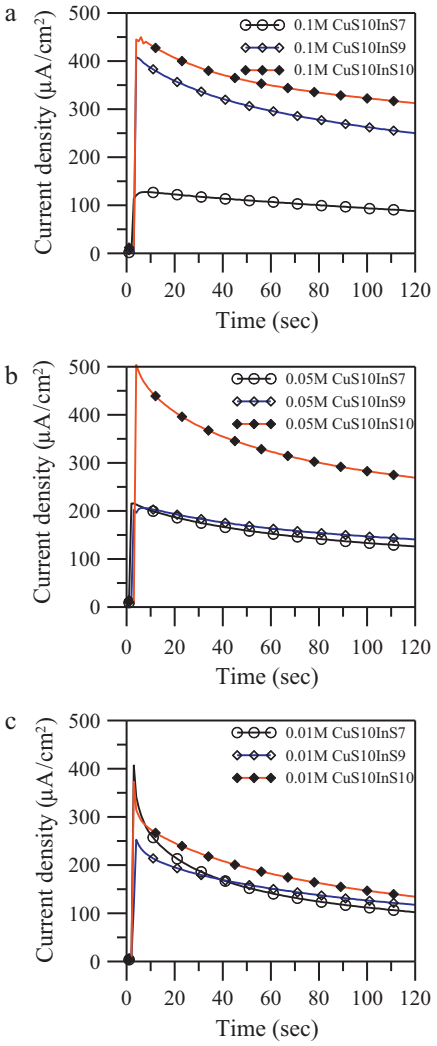

Fig. 7. Current density as a function of the measurement time under visible light illumination with 100 mW/cm^2 intensity for different precursor concentrations at fixed deposition cycles of CuS10 and InS7–10, (a) 0.1 M, (b) 0.05 M, (c) 0.01 M.

the segregation of second phases and peeling off CIS nanoparticles.

However, the thickness of CIS layer varied with the uneven morphology of TiO_2 nanotubes surface. Additionally, inhomogeneous coverage also affected the thickness identification clearly. Therefore, it is difficult to observe the thickness directly and exactly. Alternatively, the precursor concentration and deposition cycles are used to present the effect of film thickness. As the presented results and discussion shown, higher precursor concentration and more deposition cycles of CuSa and InSb could increase the deposition thickness of CIS layer. Nevertheless, the thickness decreased if too high precursor concentration and too more deposition cycles due to peeling off CIS nanoparticles. The optimal thickness was obtained around 0.05 M precursor concentration to reach the high peak current density, as shown in Fig. 8(a). The stable current densities after visible light illumination increased with the InSb deposition cycles increase for the 0.05 M CuS10InSb but not for 0.05 M CuS20InSb, as shown in Fig. 8(b). Therefore, this informed that the suitable thickness could be completed to achieve the well crystallinity, coverage and high photosensitivity of CIS by combining the precursor concentration with deposition cycles. The obtained high current density indicated an n-type CIS with a lower band gap (<1.5 eV for a single crystal CIS) extending the absorption of the large solar spectrum into the infra-red range. It demonstrates

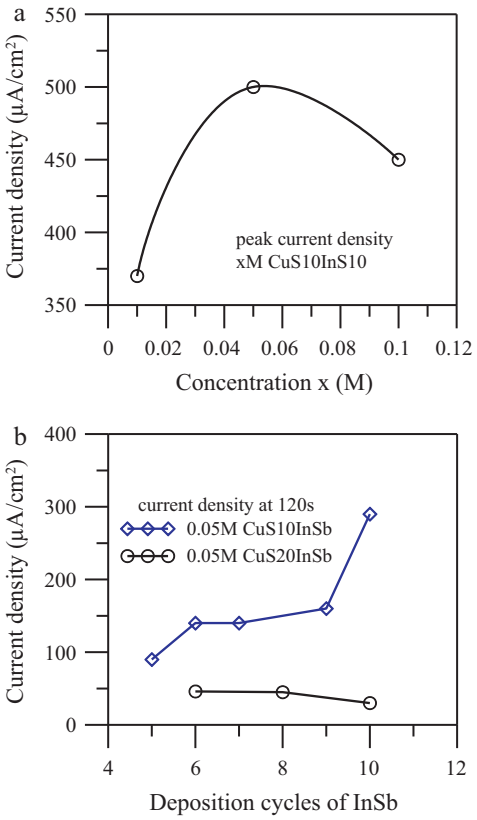

Fig. 8. Current density as a function of (a) the precursor concentration and (b) the deposition cycles of InSb for 0.05 M CuS10InSb and 0.05 M CuS20InSb.

the inorganic CIS potentially instead of organic dye to use in photosensitive solar cells by simple ICLR process.

4. Conclusions

The annealed TiO_2 nanotube arrays (TNAs) of anatase with high crystallinity and nano-sized grains as well as a high surface area exhibited a high photocatalytic efficiency. The photocurrent density of the TiO_2 modified TNAs (T-TNAs) is higher than that of the TNAs only annealed without TiO_2 modification under UV illumination, but no photocurrent was detected for either TNAs or T-TNAs under visible light illumination. The photosensitive response to visible light is really the photosensitivity of $CuInS_2$ (CIS) after subsequent CIS coating. The CIS layers on the T-TNAs comprised nano-spherical particles less than 20 nm in size produced by the ICLR method.

The nucleation and growth of the CIS nanoparticles proceeded along the edge of the top open hole of the nanotubes forming a crater-like shape, and then extended over the tubes surface as the precursor concentration and number of deposition cycles increased. More deposition cycles of indium sulfide were required to react with copper sulfide to reach a constant Cu/In ratio for different precursor concentrations of CuS10. The constant Cu/In (<1) ratio exhibits In-rich CIS. The number of deposition cycles of InSb is not necessarily equal to the number of deposition cycles of CuSa for stoichiometric CIS, for example, 0.05 M CuS10InS7 for Cu/In ~ 1 means that copper is lost during the InSb deposition. Stoichiometric $CuInS_2$ could be obtained approximately by controlling the precursor concentration and deposition cycles of the ICLR process. Increasing the number of deposition cycles of CuSa and InSb could increase the crystallinity of the CIS but incur a second phase occurrence. The precursor concentration and deposition cycles need to be controlled with film thickness suitably to obtain good crystallinity of the CIS and n-type of semiconductivity to achieve a high current density. A high current density of at least 300 $\mu A/cm^2$ could be achieved under visible light illumination intensity of 100 mW/cm^2. Such a high current density indicated an n-type CIS with a lower band gap (<1.5 eV for a single crystal CIS) extending the absorption of the large solar spectrum into the infra-red range. The results indicate the inorganic CIS could be instead of organic dye using in photosensitive solar cells.

Acknowledgements

The authors would like to thank the National Science Council, Taiwan, ROC for financially supporting this research under Grant No. NSC 98-2221-E-019-010. The authors also acknowledge the funding support from Grant No. A354DB2410 of Industrial Technology Research Institute, Taiwan, ROC.

References

[1] M.G. Panthani, V. Akhavan, B. Goodfellow, J.P. Schmidtke, L. Dunn, A. Dodabalapur, P.F. Barbara, B.A. Korgel, J. Am. Chem. Soc. 130 (2008) 16770–16777.
[2] B. Tell, J.L. Shay, H.M. Kasper, Phys. Rev. B 4 (1971) 2463–2471.
[3] T. Sebastian, M. Gopinath, C. Sudha Kartha, K.P. Vijayakumar, T. Abe, Y. Kashiwaba, Sol. Energy 83 (2009) 1683–1688.
[4] M.K. Agarwal, P. Patel, D.H. Chaki Sunil, D. Lakshminarayana, Bull. Mater. Sci. 21 (4) (1998) 291–295.
[5] M. Krunks, O. Kijatkina, H. Rebane, I. Oja, V. Mikli, A. Mere, Thin Solid Films 403–404 (2002) 71–75.
[6] T.T. John, M. Mathew, C.S. Kartha, K.P. Vijayakumar, T. Abe, Y. Kashiwaba, Sol. Energy Mater. Sol. Cells 89 (1) (2005) 27–36.
[7] H.J. Lewerenz, Sol. Energy Mater. Sol. Cells 83 (4) (2004) 395–407.
[8] F.M. Courtel, R.W. Paynter, B. Marsan, M. Morin, Chem. Mater. 21 (2009) 3752–3762.
[9] B. Marsen, L. Steinkopf, A. Singh, H. Wilhelm, I. Lauermann, T. Unold, R. Scheer, H.W. Schock, Sol. Energy Mater. Sol. Cells 94 (2010) 1730–1733.
[10] D.Y. Lee, J.H. Kim, Thin Solid Films 518 (2010) 6537–6541.
[11] J. Álvarez-García, B. Barcones, A. Pérez-Rodríguez, A. Romano-Rodríguez, J.R. Morante, A. Janotti, S.H. Wei, R. Scheer, Phys. Rev. B 71 (054303) (2005) 1 (9 pp.).
[12] S.T. Connor, C.M. Hsu, B.D. Weil, S. Aloni, Y. Cui, J. Am. Chem. Soc. 131 (2009) 4962–4966.
[13] K. Nose, Y. Soma, T. Omata, S. Otsuka-Yao-Matsuo, Chem. Mater. 21 (2009) 2607–2613.
[14] B. Koo, R.N. Patel, B.A. Korgel, Chem. Mater. 21 (2009) 1962–1966.
[15] S.L. Castro, S.G. Bailey, R.P. Raffaella, K.K. Banger, A.F. Hepp, J. Phys. Chem. B 108 (2004) 12429–12435.
[16] J. Xiao, Y. Xie, R. Tang, Y.J. Qian, J. Solid State Chem. 161 (2001) 179–183.
[17] S.J. Peng, F.Y. Cheng, J. Liang, Z.L. Tao, J. Chen, J. Alloys Compd. 481 (2009) 786–791.
[18] X.L. Gou, F.Y. Cheng, Y.H. Shi, L. Zhang, S.J. Peng, J. Chen, P.W. Shen, J. Am. Chem. Soc. 128 (2006) 7222–7229.
[19] J.S. Gardner, E. Shurdha, C.M. Wang, L.D. Lau, R.G. Rodriguez, J.J. Pak, J. Nanopart. Res. 10 (2008) 633–641.
[20] J.J. Nairn, P.J. Shapiro, B. Twamley, T. Pounds, R. Wandruszka, T.R. Fletcher, M. Williams, C. Wang, M.G. Norton, Nano Lett. 6 (2006) 1218–1223.
[21] P. Bera, S.I. Seok, J. Solid State Chem. 183 (2010) 1872–1877.
[22] F.M. Courtel, A. Hammami, R. Imbeault, G. Hersant, R.W. Paynter, B. Marsan, M. Morin, Chem. Mater. 22 (2010) 3752–3761.
[23] J.M. Macak, P. Schmuki, Electrochim. Acta 52 (2006) 1258–1264.
[24] R. O'Hayre, M. Nanu, J. Schoonman, A. Goossens, Nanotechnology 18 (2007) 055702 (7 pp.).
[25] M. Nanu, J. Schoonman, A. Goossens, Adv. Mater. 16 (5) (2004) 453–456.
[26] W.T. Sun, Y. Yu, H.Y. Pan, X.F. Gao, Q. Chen, L.M. Peng, J. Am. Chem. Soc. 130 (2008) 1124–1125.
[27] R. Sharma, S. Shim, R.S. Mane, T. Ganesh, A. Ghule, G. Cai, D.H. Ham, S.K. Min, W. Lee, S.H. Han, Mater. Chem. Phys. 116 (2009) 28–33.
[28] H.M. Pathan, C.D. Lokhande, Appl. Surf. Sci. 239 (2004) 11–18.
[29] Y. Shi, Z.G. Jin, C.Y. Li, H.S. An, J.J. Qiu, Appl. Surf. Sci. 252 (2006) 3737–3743.
[30] S.D. Sartale, C.D. Lokhande, Mater. Chem. Phys. 65 (2000) 63–67.
[31] M. Ristov, G.J. Saindinovski, I. Grozdanov, Thin Solid Films 123 (1985) 63–67.